Discretized light-cone quantization: $e^+e^-(\gamma)$ model for positronium

M. Kaluža
Max-Planck-Institut für Kernphysik, Postfach 103980, W-6900 Heidelberg 1, Germany and Center for Applied Mathematics and Theoretical Physics, University of Maribor, Krekova 2, YU-62000 Maribor, Slovenia, Yugoslavia

H. C. Pauli
Max-Planck-Institut für Kernphysik, Postfach 103980, W-6900 Heidelberg 1, Germany
(Received 3 September 1991)

The method of discretized light-cone quantization is applied to gauge theory in 3+1 dimensions and tested by calculating the spectrum and the wave functions for positronium. Working in a Fock-space expansion, only the electron-positron and the electron-positron-photon states are included. The light-cone Hamiltonian matrix is constructed blockwise, and diagonalized using the Bauer-Rutishauser simultaneous iteration algorithm for sparse matrices. At the current level of accuracy of about 10%, the model reproduces the binding energy and the charge radius of the positronium ground state for the coupling constant of $\alpha = 0.3$. The distribution functions for fermions and photons are presented for the ground state. In addition the light-cone Schrödinger equation has been solved.

PACS number(s): 11.15.Tk, 12.20.Ds

I. INTRODUCTION

The method of discretized light-cone quantization (DLCQ) was introduced recently [1] as a general method of solving field theories. It was successfully applied to (1+1)-dimensional models, such as quantum electrodynamics [2,3], the ϕ^4 model [4], quantum chromodynamics [5–7], and the Yukawa model [8,9]. The vacuum sector of the Schwinger model can be treated separately [10,11]. The general motivation for quantizing on the light cone is a simple calculation of observables, such as structure functions, from the light-cone wave functions [12].

To test the method of DLCQ on $(3+1)$-dimensional gauge theories, quantum electrodynamics was chosen. Most of the formalism is already published [13]. Particularly positronium has become an important testing ground for the method. The variational method used by Tang [14] as well as the two-body effective potential method used by Krautgärtner, Pauli, and Wölz [15] have been employed recently. In both approaches one has restricted to e^+e^- and $e^+e^-\gamma$ Fock states, and, despite some *ad hoc* assumptions, Ref. [15] reproduces even the hyperfine splitting. In the present work one uses the same model with just the e^+e^- and $e^+e^-\gamma$ Fock states, but it is only here that a direct diagonalization of the Hamiltonian matrix [16] is actually done. The estimate of Ref. [14] that the number of Fock states needed for reasonable answers is of the order of 10^7 will be shown to be much too pessimistic.

Actually, when considering this model in QED, one also solves the corresponding model in QCD. The $q\bar{q}$ and $q\bar{q}g$ Fock states are set up in color-neutral representations. Also the QCD Hamiltonian is color neutral and the color algebra [16] reduces to a calculation of the group invariants. In the model presented here, one simply replaces the fine-structure constant α by $\frac{4}{3}\alpha_s$ in QCD. After this work was completed, we learned about the work of Hollenberg *et al.* [17]. They use the same major model assumption as we do, namely, the exchange of at most a single boson in a fermion-antifermion system in the framework of QCD.

The so-called *gauge principle* [13,14] for the light-cone gauge is used consistently in the model. The principle demands that the real particle exchange transferring a certain momentum always has to be allowed simultaneously with the instantaneous particle-exchange matrix element, to which the same momentum transfer can be ascribed. The way in which the principle works for the instantaneous and real-*photon* exchange was shown already on an example of the light-cone Schrödinger equation [12, 14]. In the model presented here, the gauge principle for the instantaneous and real photon exchange is realized by employing the appropriate regulator in the $e^+e^-\gamma$ space. An important property of the regulator used is that it retains all the instantaneous photon interaction matrix elements between the e^+e^- states, in contrast with the regulator of Ref. [14]. The instantaneous *fermion* interaction piece of the Hamiltonian is included in our model, in accordance with the gauge principle. This was not the case in the similar approaches mentioned above [14, 15].

Solving the model, to be referred to as the $e^+e^-(\gamma)$ model, we face a sizable six-dimensional momentum-space problem, augmented by the spin degrees of freedom. To cope with the problem, we devise and apply sparse Hamiltonian matrix techniques and make use of the exact discrete symmetries. We employ the counterterm approach of Tang, Brodsky, and Pauli [13] for the fermion self-mass to normalize the invariant-mass-

squared ionization threshold in the positronium sector to the value of $4m^2$ where m is the Lagrangian electron mass.

One of the purposes of this work is to investigate the question of whether the nonperturbative relativistic three-body problem for positronium is tractable with the present technology, using DLCQ. We concentrate on the positronium ground state and investigate the degree of independence of the invariant mass squared, the charge radius, and the probability of finding the e^+e^- state in the positronium, on all mathematical parameters at a fixed value of the coupling constant $\alpha = 0.3$. The positronium structure function and the photon distribution function of positronium at a coupling constant $\alpha = 0.3$ are presented. The coupling constant is fixed to $\alpha = 0.3$ throughout this paper. This value is a compromise between the very small physical value of $\alpha \approx 1/137$ where the eigenvalues deviate from the ionization threshold $4m^2$ by uncomfortably small amounts, and the larger values, where the models presented here will fail.

Before solving the $e^+e^-(\gamma)$ model we will present a solution to the light-cone Schrödinger equation for positronium. Using this example we show the importance of the Coulomb counterterm [15, 16] and discuss two possible regulators in $e^+e^-\gamma$ space. In the $e^+e^-(\gamma)$ model the problem of the *zero-mode* photon exchange in the light-cone Hamiltonian and the Coulomb singularity problem are solved in the same way as in the light-cone Schrödinger equation.

The method presented here is potentially able to test the *ad hoc* assumptions of the two-body effective potential method [12, 15]. If these assumptions prove correct then this will motivate the use of the effective potential method in the $e^+e^-(\gamma)$ model. Thus, it will be possible to treat the four-body problem using the present technology. This will enable treatment of the two-photon exchange between the fermion and the antifermion. The nonperturbative calculation of the Lamb shift and the Uehling term in QED as well as the calculation of the first non-Abelian effects in heavy quarkonia in QCD will become feasible, using the light-cone techniques.

II. THE MODEL

The formalism for QED using the DLCQ method has been described in Refs. [13, 14, 16]. Here we merely present the expansion of the wave function and give the active parts of the QED Hamiltonian for the sake of completeness.

A. Positronium wave function

As the main assumption of the model, the full positronium (Ps) wave function is truncated to contain just the contributions of the e^+e^- and the $e^+e^-\gamma$ Fock states

$$|\,\mathrm{Ps}\rangle = \sum_{x\,k_\perp\lambda_1\lambda_2} \psi^{e^+e^-}_{\lambda_1\lambda_2}(x,k_\perp) b^\dagger_{x,k_\perp,\lambda_1} d^\dagger_{1-x,-k_\perp,\lambda_2}\,|\,0\rangle + \sum_{\substack{x_1 k_{\perp1} x_2 k_{\perp2}\\ \lambda_1\lambda_2\lambda_3}} \psi^{e^+e^-\gamma}_{\lambda_1\lambda_2\lambda_3}(x_1,k_{\perp1},x_2,k_{\perp2}) b^\dagger_{x_1 k_{\perp1}\lambda_1} d^\dagger_{x_2 k_{\perp2}\lambda_2} a^\dagger_{1-x_1-x_2,-k_{\perp1}-k_{\perp2},\lambda_3}\,|\,0\rangle. \tag{1}$$

Positronium, as viewed in the $e^+e^-(\gamma)$ model, is depicted in Fig. 1. The single-photon exchange, enabled by the existence of the $e^+e^-\gamma$ state should provide the Bohr-Sommerfield physics, such as fine and hyperfine splittings. By not allowing the single-photon (γ) and the two-photon ($\gamma\gamma$) Fock states in our basis, the effects connected with the pair annihilation are neglected. By not considering the $e^+e^-e^+e^-$ states, the Uehling vacuum-polarization terms are absent. By not considering the $e^+e^-\gamma\gamma$ states, the vertex correction part of the Lamb shift is missing while the part coming from the fermion self-energy is there.

The positronium system is put into a box of the size $2L$ in the longitudinal direction and $2L_\perp$ in the perpendicular directions. With the antiperiodic boundary conditions the longitudinal-momentum fractions x, x_1, and x_2 in Eq. (1) assume discrete values $1/K$, $3/K$, $5/K,\ldots,(K-1)/K$ where the even integer K is called the longitudinal resolution. The perpendicular momenta $k_\perp$, $k_{\perp1}$, and $k_{\perp2}$ assume the values $0, \pm\pi/L_\perp, \pm2\pi/L_\perp, \ldots$. The particles carry two physical spin projections, so $\lambda_{1,2} = \pm\frac{1}{2}$ and $\lambda_3 = \pm1$. The light-cone quantization approach is frame independent, and for convenience we choose to work in the frame in which the system has total longitudinal momentum $P^+ = K(2\pi/L)$ and total perpendicular momentum $P_\perp$ equal to zero. The discretization rendered the Fock basis countable and the ultraviolet regularization to be presented below will render it finite.

B. Active part of the Hamiltonian

The light-cone Hamiltonian is defined as a mass squared operator

$$H_{\mathrm{LC}} = P^+P^- - P_\perp^2 \tag{2}$$

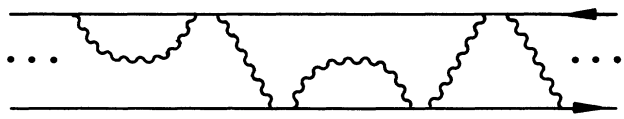

FIG. 1. Light-cone time evolution of positronium in the $e^+e^-(\gamma)$ model. Positronium can be either in an e^+e^- or in an $e^+e^-\gamma$ state. The photon emitted from the fermion can either be absorbed by the same fermion or by the antifermion. Each particle line spanning a single time interval represents either a real or an instantaneous particle.

TABLE I. QED Hamiltonian terms, active in the $e^+e^-(\gamma)$ model. The $b_q^\dagger$, $d_q^\dagger$, and $a_q^\dagger$ are creation operators for positron, electron, and photon, respectively. The symbol H.c. stands for Hermitian conjugate. Each particle carries a longitudinal-momentum fraction x, a perpendicular momentum $k_\perp$, and a spin projection λ, compiled in $q = (x, k_\perp, \lambda) = (\mathbf{k}, \lambda)$. The fine-structure constant α appears in the parameter $\beta = (\alpha/2\pi^2)(2/K)(\pi/L_\perp)^2$. The photon polarization vectors are $\epsilon_\perp(\lambda) = -(1/\sqrt{2})(\lambda, i)$, with $\lambda = \pm 1$. The regulator is $R(x, k_\perp) = \Theta((m^2 + k_\perp^2)/x(1-x) \leq 4m^2 + \Lambda^2)$.

H_0	=	$\sum_q \left((b_q^\dagger b_q + d_q^\dagger d_q) \frac{m^2 + k_\perp^2}{x} + a_q^\dagger a_q \frac{k_\perp^2}{x} \right)$
$V_{e\to e\gamma}$	=	$\sqrt{\beta} \sum_{q_1 q_2 q_3} (b_{q_1}^\dagger b_{q_2} a_{q_3} - d_{q_1}^\dagger d_{q_2} a_{q_3}) \left[\delta_{\lambda_2}^{-\lambda_1} \delta_{2\lambda_2}^{-\lambda_3} \left(\frac{1}{x_2} - \frac{1}{x_1} \right) m + \delta_{\lambda_1}^{\lambda_2} \left(\frac{k_{\perp 3}}{x_3} - \delta_{\lambda_3}^{-2\lambda_1} \frac{k_{\perp 1}}{x_1} - \delta_{\lambda_3}^{2\lambda_1} \frac{k_{\perp 2}}{x_2} \right) \epsilon_\perp(\lambda_3) \sqrt{2} \right] \times \frac{1}{\sqrt{x_3}} \delta^3_{\mathbf{k}_1, \mathbf{k}_2 + \mathbf{k}_3} + \text{H.c.}$
$S^{(s)}_{ee\to ee}$	=	$\beta \sum_{q_1 q_2 q_3 q_4} b_{q_1}^\dagger b_{q_2} d_{q_3}^\dagger d_{q_4} \delta_{\lambda_1}^{\lambda_2} \delta_{\lambda_3}^{\lambda_4} \frac{-2}{(x_2 - x_1)^2} \delta^3_{\mathbf{k}_1 + \mathbf{k}_3, \mathbf{k}_2 + \mathbf{k}_4}$
$S^{(a)}_{e\gamma\to e\gamma}$	=	$\beta \sum_{q_1 q_2 q_3 q_4} (b_{q_1}^\dagger b_{q_2} a_{q_3}^\dagger a_{q_4} + d_{q_1}^\dagger d_{q_2} a_{q_3}^\dagger a_{q_4}) \delta_{\lambda_3}^{\lambda_4} \delta_{\lambda_1}^{\lambda_2} \delta_{\lambda_4}^{-2\lambda_1} \frac{1}{x_2 + x_4} \frac{1}{\sqrt{x_3 x_4}} \delta^3_{\mathbf{k}_1 + \mathbf{k}_3, \mathbf{k}_2 + \mathbf{k}_4}$
$L_{e\to e}$	=	$\sum_q (b_q^\dagger b_q + d_q^\dagger d_q) \frac{\delta m_1^2 + \delta m_2^2}{x}$
δm_1^2	=	$\beta \sum_{q'} \left(\frac{1}{1-y} + \frac{2}{y^2} - \frac{2m^2}{m^2 y^2 + (l_\perp - y k_\perp)^2} \right) R(x(1-y), k_\perp - l_\perp)$
δm_2^2	=	$-S_2^2/(1 - S_1)$
		$S_1 = -\beta \sum_{q'} \frac{(1-y)}{m^2 y^2 + (l_\perp - y k_\perp)^2} R(x(1-y), k_\perp - l_\perp)$
		$S_2 = -\beta \sum_{q'} \frac{my}{m^2 y^2 + (l_\perp - y k_\perp)^2} R(x(1-y), k_\perp - l_\perp)$

with the light-cone momenta $P^\pm = P^0 \pm P^3$, and is derived canonically from the QED Lagrangian [14, 16, 18, 19], using the light-cone time in place of the usual time and choosing the light-cone gauge $A^+ = 0$. We emphasize that the restriction to the e^+e^- and $e^+e^-\gamma$ Fock spaces together with the so-called *gauge principle* [13, 14] determines the active part of the light-cone Hamiltonian.

The full Hamiltonian contains many different types of interactions (graphs). As a part of the model assumptions, many of them are omitted either because their matrix elements are zero in our Fock basis, or because of the gauge principle. The remaining, active part of the Hamiltonian is thus

$$H_{\rm LC} = H_0 + V_{e\to e\gamma} + S^{(s)}_{ee\to ee} + S^{(a)}_{e\gamma\to e\gamma} + L_{e\to e} \qquad (3)$$

with the explicit expressions given in Table I. The free part H_0 is independent of the coupling constant and is diagonal in the Fock-space representation. The vertex interaction $V_{e\to e\gamma}$ connects the e^+e^- and the $e^+e^-\gamma$ Fock spaces, and is graphically represented in Fig. 2(a). The instantaneous photon interaction $S^{(s)}_{ee\to ee}$ can be visualized as the exchange of an instantaneous photon as in Fig. 2(b). According to the gauge principle, the instantaneous photon interaction should be included only if the real-photon exchange is present as well. Therefore, the instantaneous photon interaction $S^{(s)}_{ee\to ee}$ is active only in e^+e^- space, since its action in $e^+e^-\gamma$ space would require the $e^+e^-\gamma\gamma$ Fock states, which are excluded in the model. Correspondingly, the instantaneous fermion interaction $S^{(a)}_{e\gamma\to e\gamma}$, represented in Fig. 2(c), should act only in $e^+e^-\gamma$ space. Finally, the fermion mass counterterm $L_{e\to e}$ from Figs. 2(d) and 2(e), to be discussed below, should be active only in e^+e^- space.

The photon emitted from the fermion can be absorbed by the same fermion, so the fermion self-mass loop appears. In the counterterm approach [13], applied here, the fermion mass counterterm $L_{e\to e}$, obtained from the perturbation theory to second order, is added to the light-cone Hamiltonian. The contribution denoted by δm_1^2 in Table I and depicted in Fig. 2(d) is negative of the one-loop fermion self-mass graph and can be understood as

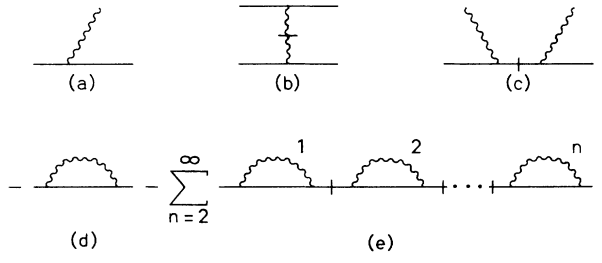

FIG. 2. Active part of the light-cone Hamiltonian in the $e^+e^-(\gamma)$ model: (a) vertex interaction; (b) instantaneous photon interaction; (c) instantaneous fermion interaction; (d) one-loop part of the fermion mass counterterm; and (e) loop-chain part of the fermion mass counterterm. For simplicity, the instantaneous fermion graphs are drawn stretched.

the instantaneous fermion and the instantaneous photon self-induced inertia contribution plus a logarithmically divergent term [16]. The latter is added for convenience since it cancels the logarithmically divergent piece of the fermion self-mass loop. The self-induced inertia contributions have to be included by the gauge principle. They are quadratically divergent with Λ and exactly cancel the quadratic divergence from the fermion self-mass loop. To cancel the fermion self-mass coming from the chains of loops connected with instantaneous fermion interaction, the fermion mass counterterm δm_2^2 contribution represented in Fig. 2(e), is added [13].

The counterterm $L_{e\to e}$ cancels all the loop corrections to the fermion self-mass [13], so that the physical fermion mass has the same numerical value as the Lagrangian fermion mass. This sets the ionization threshold in invariant mass squared M^2 to $4m^2$, where m is the Lagrangian fermion mass.

C. Regulating the Fock space

In the first step, the e^+e^- Fock space is regulated by limiting the invariant mass squared of the e^+e^- states $M^2_{e^+e^-}$:

$$\frac{m^2+k_\perp^2}{x(1-x)} \le 4m^2+\Lambda^2, \tag{4}$$

with the notation of Eq. (1). The regulator is completely equivalent to the Brodsky-Lepage [12] regulator $(m^2+k_\perp^2)/x(1-x) \le \Lambda^2_{\rm BL}$, but for the redefinition $\Lambda^2_{\rm BL} = 4m^2+\Lambda^2$. In the second step, the $e^+e^-\gamma$ Fock space is regulated. In principle one could regulate the $e^+e^-\gamma$ space by demanding that the free invariant mass squared of the Fock state $M^2_{e^+e^-\gamma}$ be less than $4m^2+\Lambda^2$, as in the e^+e^- space. For reasons to become clear below, we have used the following regulator in $e^+e^-\gamma$ space. The $e^+e^-\gamma$ state $b^\dagger_{q_1}d^\dagger_{q_2}a^\dagger_{q_3}\mid 0\rangle$ is included in the Fock basis if and only if the two regulating conditions

$$\frac{m^2+k_{\perp 2}^2}{x_2(1-x_2)} \le 4m^2+\Lambda^2 \quad\text{and}\quad \frac{m^2+k_{\perp 3}^2}{x_3(1-x_3)} \le 4m^2+\Lambda^2 \tag{5}$$

are satisfied, with the notation $q_i=(x_i,k_{\perp i})$ of Fig. 3(a). The regulator thus allows precisely for those $e^+e^-\gamma$ basis states, for which the instantaneous photon-exchange diagram is possible [16], with momenta assignments as in Fig. 3(a). The regulator is thus in accord with the gauge principle.

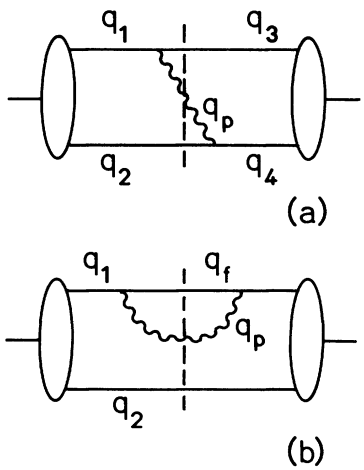

FIG. 3. Regulating the $e^+e^-\gamma$ Fock space. (a) The Fock state $b^\dagger_{q_3}d^\dagger_{q_2}a^\dagger_{q_p}\mid 0\rangle$ is in the $e^+e^-\gamma$ Fock basis, if and only if the corresponding e^+e^- Fock states $b^\dagger_{q_1}d^\dagger_{q_2}\mid 0\rangle$ and $b^\dagger_{q_3}d^\dagger_{q_4}\mid 0\rangle$ are included. (b) The allowed $e^+e^-\gamma$ Fock states specify also the loop momenta q_f and q_p.

Having specified the allowed momentum space of the e^+e^- states and the $e^+e^-\gamma$ states, the allowed momenta of the loop graph of Fig. 3(b) are specified. The fermion momenta q_2 and q_f are regulated by the conditions of Eqs. (5), where q_3 is replaced by q_f. The notation is $q_i=(x_i,k_{\perp i})$. The photon momentum q_p is regulated automatically by the momentum conservation.

D. Treatment of zero-mode photon states

The light-cone Hamiltonian as given in Table I seems to present a problem to the extent that the free, the vertex, and the instantaneous interaction matrix elements are all singular when the particles have a vanishing longitudinal-momentum fraction x. For convenience we call them *zero-mode* particles.

A prescription for the treatment of the zero-mode photons, used in Ref. [20], which was motivated by the Leibbrandt-Mandelstam prescription [21], leads to an inefficient procedure when applied to positronium [14, 16]. Guided by the light-cone Schrödinger equation, to be presented below, we find it more efficient to use the following procedure. First, one discards all the $e^+e^-\gamma$ Fock states with zero-mode photons. Second, in the formally infinite matrix element of the instantaneous photon interaction $S^{(s)}_{ee\to ee}$ one substitutes

$$\left.\frac{1}{(x_2-x_1)^2}\right|_{x_2=x_1} \to \frac{1}{(k_{\perp 2}-k_{\perp 1})^2/4m^2}, \tag{6}$$

where $(x_2-x_1, k_{\perp 2}-k_{\perp 1})$ are momentum quantum numbers of the instantaneous photon. Thus, the zero-mode photon exchange is treated as an effective Coulomb interaction, like in the light-cone Schrödinger equation, see Eq. (13). Note that both the instantaneous photon interaction and the effective Coulomb interaction conserve spin. The effective Coulomb interaction for zero-mode photons contains a contribution from the discarded real exchanged photons as well as a contribution from the instantaneous photon interaction. In the case $x_2-x_1=0$, $k_{\perp 2}-k_{\perp 1}=0$, the matrix element is still formally infinite and is set to zero by hand.

E. Treatment of Coulomb singularity

The case $x_2-x_1=0$, $k_{\perp 2}-k_{\perp 1}=0$ is nothing but the Coulomb singularity in light-cone momentum representation which is taken care of by introducing the Coulomb counterterm, taken from the light-cone Schrödinger equa-

tion [22, 15, 16, 23, 24]. The Coulomb counterterm operator, which acts only in the e^+e^- space, can be formally written as

$$C_c = \sum_q b_q^\dagger b_q [C_i(x, k_\perp) - C_s(x, k_\perp)], \tag{7}$$

where $q = (x, k_\perp, \lambda)$ and

$$C_i(x, k_\perp) = -\frac{\alpha}{\pi^2} \int_0^1 dx' d^2k'_\perp \frac{R(x', k'_\perp)}{(x' - x)^2 + (k'_\perp - k_\perp)^2/4m^2} \tag{8}$$

and

$$C_s(x, k_\perp) = -\frac{\alpha}{\pi^2} \frac{2}{K} \left(\frac{\pi}{L_\perp}\right)^2 \sum_{\mathbf{k}' \neq \mathbf{k}} \frac{R(x', k'_\perp)}{(x' - x)^2 + (k'_\perp - k_\perp)^2/4m^2}. \tag{9}$$

The regulator R restricts the summation over the discrete points $\mathbf{k}' = (x', k'_\perp)$, admitted by Eq. (4). The same regulator is used in the integral for C_i above. The $k'_\perp$ integration in $C_i(x, k_\perp)$ in Eq. (8) is done analytically, and the one-dimensional integration over x' is performed numerically with high precision. Note that the Coulomb counterterm vanishes in the continuum limit and is added for purpose of faster convergence with K and $L_\perp$.

This completes the definition of the $e^+e^-(\gamma)$ model. The Fock basis states $\{|\,\phi_j\rangle\}$ and the active part of the QED light-cone Hamiltonian $H_{\rm LC}$ have been specified. The eigenstates $|\,\psi\rangle$ in the Fock basis $\{|\,\phi_j\rangle\}$ will be calculated by diagonalizing the Hamiltonian matrix

$$\sum_j \langle\phi_i \mid H_{\rm LC} \mid \phi_j\rangle\langle\phi_j \mid \psi\rangle = M^2 \langle\phi_i \mid \psi\rangle, \tag{10}$$

which will be referred to as solving the $e^+e^-(\gamma)$ equation.

F. Light-cone Schrödinger equation

For reason of comparison with the results of the $e^+e^-(\gamma)$ equation we will study also the light-cone Schrödinger (LCS) equation results. In particular, it is possible to compare the eigenvalues of the LCS equation and the $e^+e^-(\gamma)$ equation at exactly the same values of parameters. The LCS equation

$$\left(M^2 - \frac{m^2 + k_\perp^2}{x(1-x)}\right) \psi(x, k_\perp) = \frac{\alpha}{\pi^2} \int_0^1 dx' \int d^2k'_\perp \frac{\psi(x', k'_\perp)}{(k_\perp - k'_\perp)^2/4m^2 - (x - x')^2} \tag{11}$$

is a nonrelativistic approximation to the full problem, as shown by Lepage and Brodsky [12]. In its discrete form, it is an eigenequation for the effective light-cone Hamiltonian of QED in positron-electron space,

$$H_{\rm eff} = H_0 + V_{\rm eff}, \tag{12}$$

where H_0 is the kinetic energy of the e^+e^- pair including their rest mass

$$H_0 = \sum_q (b_q^\dagger b_q + d_q^\dagger d_q) \frac{m^2 + k_\perp^2}{x}$$

and $V_{\rm eff}$ is the effective potential energy:

$$V_{\rm eff} = -\beta \sum_{q_1 q_2 q'_1 q'_2} b_{q_1}^\dagger b_{q_2} d_{q'_2}^\dagger d_{q'_1} \frac{2\delta_{\lambda_1}^{\lambda_2} \delta_{\lambda'_1}^{\lambda'_2}}{(k_{\perp 2} - k_{\perp 1})^2/4m^2 + (x_2 - x_1)^2} \delta_{\mathbf{k}_1 + \mathbf{k}'_2, \mathbf{k}_2 + \mathbf{k}'_1}. \tag{13}$$

Here q stands for momenta and spin projection $q = (\mathbf{k}, \lambda) = (x, k_\perp, \lambda)$ and

$$\beta = \frac{\alpha}{2\pi^2} \frac{2}{K} \left(\frac{\pi}{L_\perp}\right)^2.$$

The LCS equation can be thought of as the usual momentum-space Schrödinger equation for positronium, written in the light-cone variables.

III. SOLVING THE MODEL ON THE COMPUTER

In the $e^+e^-(\gamma)$ model we are dealing with a sizable, six-dimensional momentum-space problem. Furthermore, each particle carries spin. One reduces the numerical complexity by using the exact discrete symmetries C, R^2, and P_x, which are the charge conjugation, the rotation about the z axis by π and the mirror symmetry with respect to the yz plane, respectively. They commute with the light-cone Hamiltonian and among themselves and are used to classify the positronium states. The Hamiltonian matrix is a sparse matrix. By calculating it blockwise, one reduces the time to calculate from $O(N^4)$ to $O(N^3)$ for the $e^+e^-(\gamma)$ model, where N is the number of the e^+e^- Fock basis states. Sparse matrix diagonalization again requires $O(N^3)$ time, to be compared to $O(N^6)$ requirement of the usual, full matrix diagonalization routines for the same model.

A. Fock space construction

The Fock space basis $\{|\,\phi_i\rangle\}$ is constructed by combining *partitions* of various quantum numbers. This enables efficient, blockwise calculation of the Hamiltonian matrix $H_{ij} = \langle\phi_i \mid H \mid \phi_j\rangle$. Given the longitudinal resolution K, which is an even number, the lookup tables $P_l^{e^+e^-}$ and $P_l^{e^+e^-\gamma}$ of all the longitudinal-momentum partitions for this K are constructed:

$$P_l^{e^+e^-} = \{(n, K-n) \mid n = 1, 3, \ldots, K-1\}$$

and (14)

$$P_l^{e^+e^-\gamma} = \{(n_1, n_2, K-n_1-n_2) \mid n_{1,2} = 1, 3, \ldots; K-n_1-n_2 > 0\}.$$

Similarly, given the transverse resolution $R_\perp$, which is defined as $R_\perp = L_\perp \Lambda/\pi$, the lookup tables $P_p^{e^+e^-}$ and $P_p^{e^+e^-\gamma}$ for the perpendicular momenta are constructed:

$$P_p^{e^+e^-} = \{(-n, n) \mid n = 0, \pm 1, \pm 2, \ldots \mid n \mid \leq R_\perp/2\}$$

and (15)

$$P_p^{e^+e^-\gamma} = \{(n_1, n_2, -n_1-n_2) \mid n_{1,2} = 0, \pm 1, \pm 2, \ldots; \mid n_{1,2} \mid \leq R_\perp/2\}.$$

The lookup tables $P_\lambda^{e^+e^-}$ and $P_\lambda^{e^+e^-\gamma}$ for spin partitions are

$$P_\lambda^{e^+e^-} = \{(\lambda_1, \lambda_2) \mid \lambda_{1,2} = \pm\tfrac{1}{2}\}$$

and (16)

$$P_\lambda^{e^+e^-\gamma} = \{(\lambda_1, \lambda_2, \lambda_3) \mid \lambda_{1,2} = \pm\tfrac{1}{2}, \lambda_3 = \pm 1\}.$$

Each Fock state $\mid \mu\rangle$ is specified by five integers, $\mid \mu\rangle = (p; p_l, p_1, p_2, p_\lambda)$. The first integer p is the particle content of the Fock state, which is either e^+e^- or $e^+e^-\gamma$. The second integer, p_l, is the longitudinal-momentum partition number. It points to a certain entry in the $P_l^{e^+e^-}$ table or in the $P_l^{e^+e^-\gamma}$ table, depending on the particle content p. Analogously, the integers p_1 and p_2 are the perpendicular momentum partition numbers and p_λ is the spin partition number.

Fock state candidates of given particle content are produced by combining the four partitions denoted by p_l, p_1, p_2, and p_λ. The first Fock state candidates in e^+e^- space are $(1;1,1,1,1)$, $(1;1,1,1,2)$, $(1;1,1,1,3)$, $(1;1,1,1,4)$, $(1;1,1,2,1),\ldots$, since there are four possible spin combinations. The regulator conditions, Eq. (4) or Eq. (5), are inspected for each Fock-space candidate. The candidates not satisfying the regulator conditions are discarded. The admitted combinations of four partitions for each particle content constitute the full Fock basis. When needed, the quantum numbers of individual particles in the Fock state are reconstructed from the partition numbers. In Table II the Fock state basis sizes are presented for some values of the resolutions and the regulator Λ.

TABLE II. Hamiltonian matrix sizes for various parameter values in the $e^+e^-(\gamma)$ model. The matrix sizes presented are full – unsymmetrized matrix sizes.

$R_\perp$	K	Λ	Matrix size
2.99	30	0.6	1316
5.99	30	0.6	17796
5.99	30	1.2	61764
5.99	62	0.6	81668

In the next step, the Fock basis of *symmetrized* Fock states is constructed. The symmetrized Fock states are the eigenstates of the discrete symmetry operators: P_x mirror symmetry operator, C charge conjugation, and R^2 rotation about the z axis by π. The symmetrized Fock state $\mid \phi_s\rangle$ is obtained from the unsymmetrized Fock state $\mid \phi\rangle$ by applying the Young projector:

$$\mid \phi_s\rangle = \mathcal{N}_s(1+\lambda_P P_x)(1+\lambda_C C)(1+\lambda_R R^2) \mid \phi\rangle, \tag{17}$$

where the λ_P, λ_C, λ_R are the discrete symmetry eigenvalues chosen. Each λ can take the values of $+1$ or -1. $\mathcal{N}_s$ is the normalization constant which ensures orthonormality of the symmetrized states, $\langle(\phi_s)_i \mid (\phi_s)_j\rangle = \delta_{ij}$. The symmetrized state is stored in memory as an array of eight unsymmetrized Fock states, together with the array of eight phases and the normalization constant. The phases come from λ_P, λ_C, and λ_R in Eq. (17) and from the discrete symmetry transformation properties of the creation operators for positrons, electrons, and photons: i.e.,

$$\begin{aligned}
&\mathcal{C} b^\dagger_{q\lambda} \mathcal{C}^\dagger = d^\dagger_{q\lambda}, \quad \mathcal{R} b^\dagger_{q\lambda} \mathcal{R}^\dagger = i^{-\lambda} b^\dagger_{\hat{q}\lambda}, \quad \mathcal{P}_x b^\dagger_{q\lambda} \mathcal{P}_x^\dagger = b^\dagger_{\tilde{q},-\lambda}, \\
&\mathcal{C} d^\dagger_{q\lambda} \mathcal{C}^\dagger = b^\dagger_{q\lambda}, \quad \mathcal{R} d^\dagger_{q\lambda} \mathcal{R}^\dagger = i^{-\lambda} d^\dagger_{\hat{q}\lambda}, \quad \mathcal{P}_x d^\dagger_{q\lambda} \mathcal{P}_x^\dagger = -d^\dagger_{\tilde{q},-\lambda}, \\
&\mathcal{C} a^\dagger_{q\lambda} \mathcal{C}^\dagger = -a^\dagger_{q\lambda}, \quad \mathcal{R} a^\dagger_{q\lambda} \mathcal{R}^\dagger = i^{-\lambda} a^\dagger_{\hat{q}\lambda}, \quad \mathcal{P}_x a^\dagger_{q\lambda} \mathcal{P}_x^\dagger = a^\dagger_{\tilde{q},-\lambda}.
\end{aligned} \tag{18}$$

Here λ represents the spin projections, and $q = (x, p_x, p_y)$. The abbreviations $\hat{q} = (x, -p_y, p_x)$ and $\tilde{q} = (x, -p_x, p_y)$ are used for convenience.

B. Calculation of the Hamiltonian matrix

The specific ordering of the Fock states, described above, gives rise to the *block structure* of the Hamiltonian matrix. In the $e^+e^-(\gamma)$ model the largest blocks are four

blocks, specified by a pair of integers $(p^{\rm bra}, p^{\rm ket})$. The integers represent the particle contents of the bra and the ket Fock states. Inside each such particle-content block there is a number of the longitudinal-momentum partition blocks, each specified by a pair of integers $(p_l^{\rm bra}, p_l^{\rm ket})$. Inside each such block there are perpendicular momentum (x direction) partition blocks, specified by a pair $(p_1^{\rm bra}, p_1^{\rm ket})$. Inside each such block there are the perpendicular momentum (y direction) blocks. The innermost blocks are the spin blocks, which are just single matrix elements.

The important feature of the Hamiltonian matrix in the $e^+e^-\gamma$ model is that most of the blocks on each level of the block structure are empty. The reason for this is the existence of *spectators* in the many-body matrix element. Consider, for instance, the $e^+ \to e^+\gamma$ part of the vertex matrix element $V_{e\to e\gamma}$ from Table I between e^+e^- bra and $e^+e^-\gamma$ ket. The electron is a spectator in this matrix element and must have identical quantum numbers in both e^+e^- and $e^+e^-\gamma$ states. If the longitudinal-momentum fractions of the electron in bra and in ket are not the same then the whole longitudinal-momentum partition block $(p_l^{\rm bra}, p_l^{\rm ket})$ will have this matrix element equal to zero.

The discrete symmetries P_x, C, and R^2 do not spoil the block structure of the Hamiltonian matrix [16]. The reason for that is that none of the symmetry operators transforms single-particle momenta in the x direction into the momenta in the y direction, or vice versa, cf. Eq. (18). For that reason, the R^2 symmetry instead of R was used.

The time to calculate the Hamiltonian matrix blockwise appears to be proportional to the number of nonzero entries instead to the number of all entries. The number of nonzero entries can be simply estimated. Consider, for instance, the $e^+ \to e^+\gamma$ part of the vertex matrix element $V_{e\to e\gamma}$ of Table I discussed above. Suppose that the resolutions K, $R_\perp$ and the regulator Λ are chosen such that there is altogether N e^+e^- Fock states. Then, the number of $e^+e^-\gamma$ states will be of order $O(N^2)$ as two instead of one particle momenta are at disposal. The total number of vertex matrix elements is thus $O(N^3)$. But most of them are zero as there is a spectator electron in the graph. One can still choose $O(N^2)$ $e^+e^-\gamma$ states in ket, but then the momentum partition of e^+e^- bra is specified by the momentum conservation. This gives only $O(N^2)$ nonzero entries. Similarly, there will be $O(N^3)$ instantaneous fermion matrix elements between pairs of $e^+e^-\gamma$ states and $O(N^2)$ instantaneous photon matrix elements between pairs of e^+e^- states.

C. Diagonalization

Each nonzero matrix element is written in a file as a pair of integers, indicating the row and the column of the matrix element, and a pair of real numbers, representing real and imaginary component of the matrix element. Blockwise calculation yields an unordered sequence of matrix elements. The file of matrix elements is then sorted, using a standard and fast sorting routine. The sorted file is read rowwise into a diagonalization program. In this program, the *sparse rowwise format* [25] is used, which reduces the storage occupied by one purely real or purely imaginary matrix element to one integer and one real memory location.

The complex matrix is expanded into a double-size real matrix. This does not increase the memory use. The double-size real sparse matrix is diagonalized using the NAG library routine F02FJF. To obtain the lowest few eigenvalues and eigenvectors, the Bauer-Rutishauser inverse simultaneous iteration [26, 27] is used by the routine. We chose to solve the corresponding sparse system of linear equations by the iterative NAG routine F04MBF, which uses the Lanczos algorithm [28]. Here the user has to provide just a matrix-by-vector multiplication subroutine.

Because of the matrix size doubling, two identical eigenvalues and two equivalent eigenvectors are obtained for each eigenstate. This does not present any problem in practice. The eigenvectors are stored on a file and reread by the Fock-space construction program, which transforms them back into the unsymmetrized form and calculates the observables from that form.

The diagonalization method chosen seems to require $O(N^3)$ time to diagonalize, where N is the number of e^+e^- Fock states. The method is certainly more complicated than the Lanczos method [3, 17], but is able to calculate both the ground state and the excited states with arbitrary precision, just by changing the shift parameter. In our case the eigenvalues were calculated to single-precision machine accuracy, which is about seven significant figures. The time to calculate the largest 81 668 by 81 668 matrix from Table II and to obtain a few lowest eigenvalues and eigenfunctions, was less than 12 CPU hours on an 1 Mflop workstation.

IV. RESULTS

All of the models discussed in Sec. II have five parameters, i.e., α, m, Λ, $R_\perp$, and K. The fine-structure constant α and the Lagrangian fermion mass m are physical parameters while the ultraviolet regulator Λ, the transverse resolution $R_\perp$, and the longitudinal resolution K are mathematical parameters. The results should not depend on the mathematical parameters.

What does one expect? To lowest order of approximation, the calculation should yield the Bohr spectrum

$$M^2 = m^2(2 - \alpha^2/4n^2)^2 \ , \ n = 1, 2, 3, \ldots \ . \tag{19}$$

The corresponding $1S$-state wave function is

$$\psi_{1S}(x, k_\perp) = \mathcal{N}\frac{1}{[1 + (k_\perp^2 + k_{||}^2)/k_B^2]^2}, \tag{20}$$

where $\mathcal{N}$ is a normalization constant, $k_B = m\alpha/2$ is the Bohr momentum and $k_{||}$ stands for $2m(x - \frac{1}{2})$. The reduced mass in positronium is $m_r = m/2$ and $k_B = \alpha m_r$. The covariant regulator $(m^2 + k_\perp^2)/x(1-x) \le 4m^2 + \Lambda^2$ is equivalent to the condition $k_\perp^2 + k_{||}^2 \le (\Lambda/2)^2$ to a good approximation. With a discretized approach one should expect that one can come close to the results of Eqs. (19) and (20) only if one has at least one mesh point inside the

momentum-space sphere with radius of one Bohr momentum, in addition to the central point at $x = \frac{1}{2}$, $k_\perp = 0$. One therefore should require

$$\Lambda/m > \alpha, \quad R_\perp > 2\Lambda/\alpha m, \quad \text{and} \quad K > 8/\alpha. \tag{21}$$

These are just estimates. The detailed study of parameter dependence should reveal the optimum values in order to reproduce the spectra.

In the sequel, the eigensolutions of the light-cone Schrödinger equation and of the $e^+e^-(\gamma)$ equation will be studied in succession.

A. Light-cone Schrödinger equation results

First we consider the solutions of the LCS equation because it is much simpler than the $e^+e^-(\gamma)$ equation. To verify the degree of independence on the mathematical parameters, we have varied all of them. In Fig. 4 we present the spectrum of the LCS equation as a function of transverse resolution $R_\perp$ at fixed values of $K = 30$ and $\Lambda = 1.0$. Since the LCS equation conserves spin, we could restrict ourselves to e^+e^- Fock states with total spin projection zero. The spectrum of invariant mass squared is presented. It includes both the bound states and the scattering states. For the bound states, the binding energy E can be calculated from the invariant mass squared M^2 using the formula $E = \sqrt{M^2} - 2m$.

Figure 4(a) shows the spectrum without using the technique of the Coulomb counterterm of Eq. (7). The formally infinite matrix element that corresponds to the situation $x_2 - x_1 = 0$, $k_{\perp 2} - k_{\perp 1} = 0$ in Eq. (13) is simply set to zero. One observes that the ground-state level is not stable with $R_\perp$, except perhaps locally in the region around $R_\perp = 6$, where the ground-state eigenvalue has a maximum. But, in this region the eigenvalues deviate substantially from the expected Bohr values, Eq. (19).

Figure 4(b) displays the results if one includes the Coulomb counterterm according to Eq. (7). As compared to Fig. 4(a) the eigenvalues seem to become stable with increasing $R_\perp$. They oscillate about the mean value of $M^2 = 3.913$ (close to the Bohr value of 3.91) with a standard deviation of $\Delta M^2 = 0.003$. For the chosen symmetry quantum numbers, the first excited state would be a $2S$ or a $2P$ state. Its invariant mass squared oscillates around the mean value of 3.968 (to be compared with the Bohr value of 3.978) with a standard deviation of 0.004. Worse precision in reproducing the excited states is to be expected, because of the nodes in the wave functions.

The calculations in Figs. 4(a) and 4(b) have been done with the regularization, equivalent to using the regulating conditions of Eq. (5) in the $e^+e^-\gamma$ sector, which in the LCS equation means simply including all the matrix elements of the effective interaction potential, Eq. (13). In Fig. 4(c), the results of yet another approach are shown. As mentioned earlier, the LCS equation can be understood as nonrelativistic approximation to the $e^+e^-(\gamma)$ equation. If there one would have regulated the $e^+e^-\gamma$ Fock space by the *global* Brodsky-Lepage regulator

$$M^2_{e^+e^-\gamma} \leq 4m^2 + \Lambda^2 \tag{22}$$

with $M^2_{e^+e^-\gamma}$ given by [see notation of Fig. 3(a)]

$$M^2_{e^+e^-\gamma} = \frac{m^2 + k^2_{\perp 3}}{x_3} + \frac{m^2 + k^2_{\perp 2}}{x_2} + \frac{(-k_{\perp 3} - k_{\perp 2})^2}{1 - x_3 - x_2} \tag{23}$$

the regulator would persist to show up in the LCS equation. This regulator was included in Fig. 4(c), together with the appropriate Coulomb counterterm. We observe nonstable behavior of all the eigenvalues but the lowest. The mass gap between the lowest and the first excited state is lost as $R_\perp$ is increased.

In Fig. 4(b) as well as in Fig. 4(c), one finds that the eigenvalues are nonmonotonical functions of $R_\perp$. What is a possible reason? In Fig. 4(a), the eigenvalues are smooth functions of $R_\perp$. As $R_\perp$ increases, the number of Fock states increases. The new states contribute to both kinetic and potential energy and their contributions apparently balance. One suspects that the Coulomb coun-

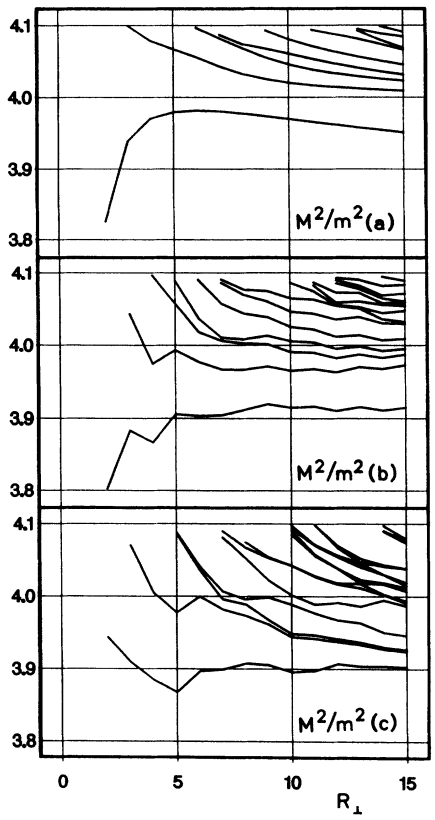

FIG. 4. Invariant-mass-squared M^2 spectrum of the LCS equation vs the transverse resolution $R_\perp$: (a) no Coulomb counterterm is included; (b) Coulomb counterterm is included, as described in the text; (c) same as (b) but with covariant regulator in the $e^+e^-\gamma$ space, see text. Calculations are done for $K = 30$, $\Lambda = 1.0$, $\alpha = 0.3$, $R_\perp = 2.0[1.0]15.0$. The symmetry quantum numbers $R^2 = +1$, $P_x = +1$, and $C = +1$ are those of the singlet 1^1S_0 ground state (parapositronium). Note the onset of convergence of the ground-state level toward the value close to the Bohr value of $M^2 = 3.91$ in (b).

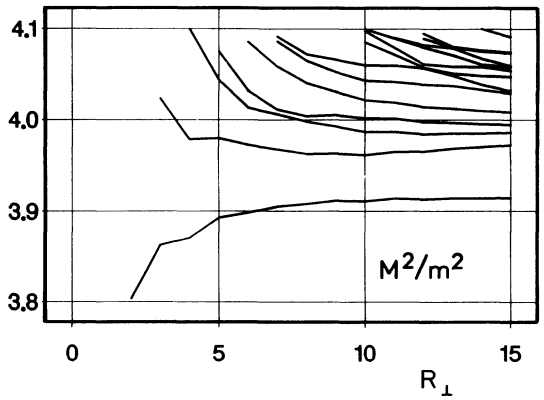

FIG. 5. Invariant-mass-squared M^2 spectrum of the LCS equation vs the transverse resolution $R_\perp$, using smoothened Coulomb counterterm, as described in the text. The calculations are done with $K = 30$, $\Lambda = 1.0$, $\alpha = 0.3$, $R_\perp = 2.0[1.0]15.0$. The symmetry quantum numbers are those of the singlet ground state (parapositronium). Note the smoother dependence on $R_\perp$ as compared to Fig. 4(b).

terterm used is a source of the nonmonotonic behavior. Indeed, the discrete part of the Coulomb counterterm, Eq. (9) is a discontinuous function of $R_\perp$. In Fig. 5, the results with the smoothened discrete part of the Coulomb counterterm are presented. The sharp cutoff

$$R(x,k_\perp) = \Theta\left(\frac{m^2+k_\perp^2}{x(1-x)} - 4m^2 - \Lambda^2\right)$$

in the discrete part of the Coulomb counterterm C_s, Eq. (9), is replaced by a smoothened one

$$R(x,k_\perp) = f\left(\left[\frac{m^2+k_\perp^2}{x(1-x)} - 4m^2 - \Lambda^2\right]/\rho^2\right), \tag{24}$$

where the sigmoid function is $f(x) = 1/(1+e^x)$ and the width ρ^2 was always chosen to be $\rho^2 = \Lambda^{3/2}m^{1/2}K^{-1/2}R_\perp^{-1/2}$. The smoothening has no impact on the mean value; the mean value of M^2 about which the ground-state eigenvalue oscillates with increasing $R_\perp$ changes only by 0.0002. However, the standard deviation decreases by a factor of 5 from 0.003 to 0.0006 and the pronounced wiggling of the eigenvalues is not present in Fig. 5. We conclude that the wiggling is caused by the Coulomb counterterm, which probably disturbs the balance between the kinetic and the potential energy. The mechanism of the wiggling is not understood in detail and should be investigated further in the future, as it interferes with the quest for precision.

B. $e^+e^-(\gamma)$ equation results

Based on the results for the LCS equation we decide to use the smoothened Coulomb counterterm also in the $e^+e^-(\gamma)$ equation, which we present in the sequel.

The $e^+e^-(\gamma)$ equation is technically much more demanding to solve as the LCS equation. The diagonalization method described in Sec. III C can in principle return the ground-state results and the results for all the excited states. Here we shall limit ourselves to study only the ground-state eigensolutions. This should reproduce the singlet ground state of the positronium (parapositronium).

It is difficult to present the whole dependence of observables on mathematical parameters. To get a flavor of the dependence, we choose the *standard set* of mathematical parameters

$$\Lambda = 0.6,\ K = 30,\ \text{and}\ R_\perp = 5.99 \tag{25}$$

and vary each of the parameters by keeping the other two constant at the standard values. Note that the standard set barely satisfies the requirements of Eq. (21) at our standard value of $\alpha = 0.3$. We shall compare the singlet

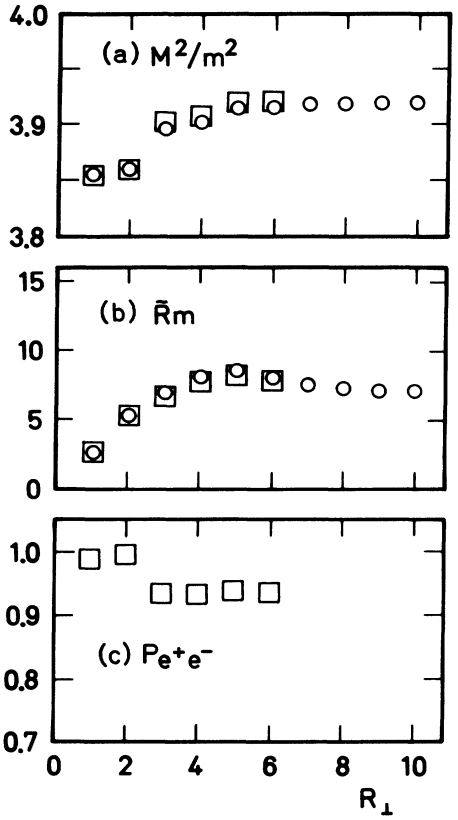

FIG. 6. Properties of the singlet ground state vs the transverse resolution $R_\perp$: (a) invariant mass squared M^2; (b) charge radius $\tilde{R}$; (c) probability $P_{e^+e^-}$ to find any e^+e^- basis state in the singlet wave function of the $e^+e^-(\gamma)$ equation. Calculations were done with $K = 30$, $\Lambda = 0.6$, $\alpha = 0.3$, $R_\perp = 0.99[1.0]5.99$ for the $e^+e^-(\gamma)$ equation (squares) and with $K = 30$, $\Lambda = 0.6$, $\alpha = 0.3$, $R_\perp = 0.99[1.0]9.99$ for the LCS equation (circles). The symmetry quantum numbers are those of the singlet ground state. The theoretical expectation for the value of M^2 including the Breit correction is 3.90. Note the onset of convergence with $R_\perp$ for all quantities for both the $e^+e^-(\gamma)$ and the LCS equation.

ground-state solution of the $e^+e^-(\gamma)$ equation with the ground-state solution of the LCS equation.

In Fig. 6(a), the invariant-mass-squared M^2 eigenvalue of the ground state is shown as a function of transverse resolution $R_\perp$ at fixed values of $K = 30$ and $\Lambda = 0.6$. One observes the onset of stabilization of M^2 with $R_\perp$ for the $e^+e^-(\gamma)$ equation (squares). More clearly, still, one sees the stabilization of M^2 for the LCS equation (circles), where more transversal points were included. The value of M^2 toward which the ground-state eigenvalue of the LCS equation tends to approach, 3.92, is above the Bohr value of about 3.91 and above the value 3.90 which includes the Breit correction. This is expected at $\Lambda = 0.6$ [16]. It is remarkable to observe that M^2 of the $e^+e^-(\gamma)$ ground state varies with $R_\perp$ in very much the same way as M^2 of the LCS equation. The $e^+e^-(\gamma)$ eigenvalues are consistently higher than the LCS values. For the two points with $R_\perp < 2$, no particle carries any transverse momentum and these points are an exception.

We also present the ground-state wave-function behavior. It is inconvenient to present the entire wave function so we rather present some of its measures. The *spin-averaged form factor* $F_1(Q^2)$ of positronium vanishes because of the charge-conjugation symmetry. By setting the electron charge to 0 and positron charge to 1 in the expression for $F_1(Q^2)$, the form factor $\tilde{F}_1(Q^2)$ is defined here as

$$\tilde{F}_1(Q^2) = \sum_{s_1 s_2} \int dx\, d^2k_\perp \psi^{e^+e^-\,*}_{s_1 s_2}(x, k_\perp + (1-x)q_\perp)\psi^{e^+e^-}_{s_1 s_2}(x, k_\perp) + \sum_{s_1 s_2 s_3} \int dx_1 d^2k_{\perp 1} dx_2 d^2k_{\perp 2} \psi^{e^+e^-\gamma\,*}_{s_1 s_2 s_3}(x_1, k'_{\perp 1}, x_2, k'_{\perp 2})\psi^{e^+e^-\gamma}_{s_1 s_2 s_3}(x_1, k_{\perp 1}, x_2, k_{\perp 2}), \tag{26}$$

with $k'_{\perp 1} = k_{\perp 1} + (1-x_1)q_\perp$ and $k'_{\perp 2} = k_{\perp 2} - x_2 q_\perp$ [29, 12]. The continuum limit notation is used. Note that $Q^2 = -q^2 = q_\perp^2$ and that $\tilde{F}_1(0)$ is normalized to 1.

The charge radius $\tilde{R}$ is interpreted as the slope of the form factor $\tilde{F}_1$ at the origin $\tilde{R}^2 = -6\partial\tilde{F}_1(Q^2)/\partial Q^2\,|_{Q^2=0}$. A convenient way to calculate the charge radius is by using the Fourier transform of the wave function [30]:

$$\tilde{R}^2_{e^+e^-(\gamma)} = R^2_{e^+e^-} + R^2_{e^+e^-\gamma}, \qquad \tilde{R}^2_{\rm LCS} = R^2_{e^+e^-} \tag{27}$$

with

$$R^2_{e^+e^-} = 3\sum_{s_1 s_2} \int dx (1-x)^2 \int d^2b_\perp b_y^2 \mid \tilde{\psi}^{e^+e^-}_{s_1 s_2}(x, b_\perp) \mid^2$$

and

$$R^2_{e^+e^-\gamma} = 3\sum_{s_1 s_2 s_3} \int dx_1 \int d^2b_{\perp 1} \int dx_2 \int d^2b_{\perp 2} [(1-x_1)b_{y1} - x_2 b_{y2}]^2 \mid \tilde{\psi}^{e^+e^-\gamma}_{s_1 s_2 s_3}(x_1, b_{\perp 1}, x_2, b_{\perp 2}) \mid^2 . \tag{28}$$

The wave functions in the perpendicular configuration space $b_\perp = (b_x, b_y)$ are Fourier transforms of the wave functions in momentum space:

$$\tilde{\psi}(x, b_\perp) = \frac{1}{2\pi} \int d^2k_\perp e^{-ik_\perp b_\perp} \psi(x, k_\perp),$$
$$\tilde{\psi}(x_1, b_{\perp 1}, x_2, b_{\perp 2}) = \frac{1}{(2\pi)^2} \int d^2k_{\perp 1} \int d^2k_{\perp 2} e^{-ik_{\perp 1}b_{\perp 1} - ik_{\perp 2}b_{\perp 2}} \psi(x_1, k_{\perp 1}, x_2, k_{\perp 2}). \tag{29}$$

In Fig. 6(b), the charge radius $\tilde{R}$ is shown as a function of transverse resolution at fixed values of $K = 30$ and $\Lambda = 0.6$. Again, one observes the onset of stabilization of $\tilde{R}$ with $R_\perp$ for the $e^+e^-(\gamma)$ equation (squares). More clearly, again, one sees the stabilization of M^2 for the LCS equation (circles), where more transversal points were included. For $R_\perp < 2$ no particle carries any transversal momentum at all, see Eq. (15). It is nevertheless interesting to see the linear growth of the charge radius $\tilde{R}$ with the transversal box size $2L_\perp = 2\pi R_\perp/\Lambda$ in Fig. 6(b) for lower values of $R_\perp$ (or $L_\perp$). Eventually, $\tilde{R}$ saturates. The transversal box size $L_\perp$ at which $\tilde{R}$ saturates, is equal to $L_\perp \approx 26m^{-1}$. It is to be compared with the limiting value of $\tilde{R}$, which is about $7m^{-1}$, as seen in Fig. 6(b). The expected value for the nonrelativistic wave function is $\tilde{R} = \sqrt{3}(m\alpha)^{-1} \approx 5.8m^{-1}$ [31]. What is the reason for such a discrepancy in the charge radius? One possible source of the discrepancy is a finite and rather small value of $\Lambda = 0.6$. With this value, the wave function is concentrated at low values of relative momentum, which makes the wave function in coordinate space broader; as we will see, the charge radius decreases with increasing Λ. An important result is that the differences between values of $\tilde{R}$ calculated with the LCS and the $e^+e^-(\gamma)$ equation in Fig. 6(b) are small at all $R_\perp$.

In Fig. 6(c) the probability $P_{e^+e^-}$ to find any e^+e^-

Fock state in the wave function

$$P_{e^+e^-} = \sum_{s_1 s_2} \int dx\, d^2k_\perp \mid \psi^{e^+e^-}_{s_1 s_2}(x, k_\perp) \mid^2 \qquad (30)$$

is shown as a function of transverse resolution at fixed values of $K = 30$ and $\Lambda = 0.6$. One observes the apparent stabilization of the $P_{e^+e^-}$ of the singlet ground state of the $e^+e^-(\gamma)$ equation with $R_\perp$. The value at which it stabilizes is $P_{e^+e^-} \approx 0.9$. The probability to find a $e^+e^-\gamma$ state in positronium is equal to $P_{e^+e^-\gamma} = 1 - P_{e^+e^-}$ in our model. The probability to find a photon state in positronium is expected to be of order of $O(\alpha^3)$ [12, 32].

In Fig. 7(a) we present the dependence of the singlet ground-state properties as functions of longitudinal resolution K at fixed $R_\perp = 5.99$ and $\Lambda = 0.6$. One observes stabilization of invariant-mass-squared eigenvalue M^2 with K, for both the $e^+e^-(\gamma)$ equation (squares) and the LCS equation (circles). The differences between the $e^+e^-(\gamma)$ equation ground-state mass squared and the LCS equation ground-state mass squared are small for each K, although they become larger with increasing K.

In Fig. 7(b), the charge radius $\tilde{R}$ is presented as a function of K. The value of $\tilde{R}$ seems to stabilize for both the $e^+e^-(\gamma)$ equation (squares) and LCS equation (circles). The charge radius of the LCS equation tends to a slightly larger value than the charge radius of the $e^+e^-(\gamma)$ equation.

In Fig. 7(c) it is seen that the $P_{e^+e^-}$ value depends strongly on K, even for larger values of K. This behavior could have been anticipated, since $P_{e^+e^-}$ is the probability to find a pair of bare electron and bare positron in positronium.

In Fig. 8, the dependence of M^2, $\tilde{R}$, and $P_{e^+e^-}$ on the last mathematical parameter, the ultraviolet regulator Λ is presented. The values of resolutions were kept fixed at $K = 30$ and $R_\perp = 5.99$. The ultraviolet regulator Λ differs from resolutions K and $R_\perp$ in that it

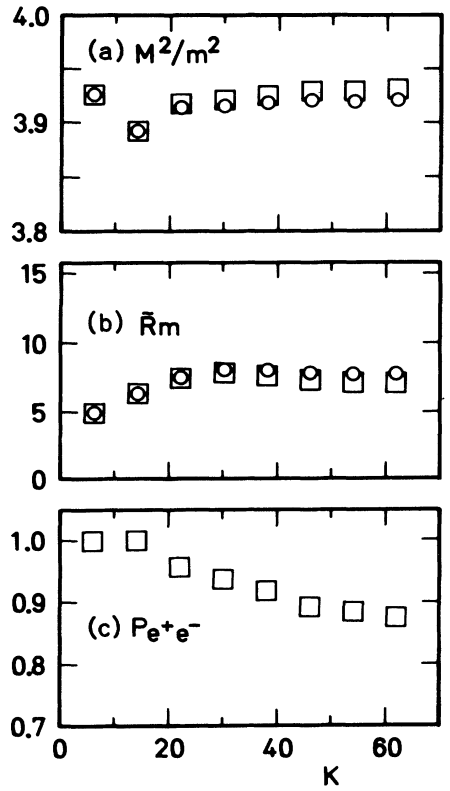

FIG. 7. Properties of the singlet ground state vs the longitudinal resolution K: (a) invariant mass squared M^2; (b) charge radius $\tilde{R}$; (c) probability $P_{e^+e^-}$ to find any e^+e^- basis state in the singlet wave function of the $e^+e^-(\gamma)$ equation. Calculations were done with $R_\perp = 5.99$, $\Lambda = 0.6$, $\alpha = 0.3$, $K = 6[8]62$ for both the $e^+e^-(\gamma)$ equation (squares) and the LCS equation(circles). The symmetry quantum numbers are those of the singlet ground state. The theoretical expectation for the value of M^2 including the Breit correction is 3.90. Note the apparent convergence with K of the invariant mass squared M^2 and of the charge radius $\tilde{R}$ for both the $e^+e^-(\gamma)$ and the LCS equation. The $P_{e^+e^-}$ does not stabilize, as opposed to the behavior with $R_\perp$ in Fig. 6.

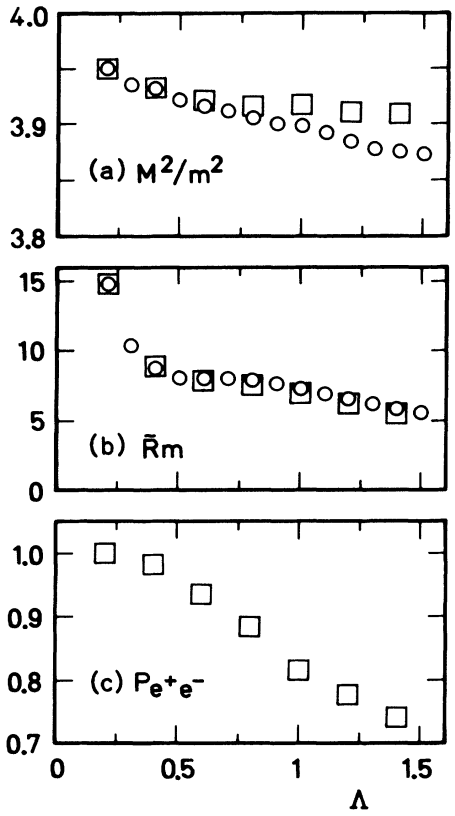

FIG. 8. Properties of the singlet ground state vs the ultraviolet regulator Λ: (a) invariant mass squared M^2; (b) charge radius $\tilde{R}$; (c) probability $P_{e^+e^-}$ to find any e^+e^- basis state in the singlet wave function of the $e^+e^-(\gamma)$ equation. Calculations were done with $R_\perp = 5.99$, $K = 30$, $\alpha = 0.3$, $\Lambda = 0.2[0.2]1.4$ for the $e^+e^-(\gamma)$ equation (squares) and with $R_\perp = 5.99$, $K = 30$, $\alpha = 0.3$, $\Lambda = 0.2[0.1]1.5$ for the LCS equation (circles). The symmetry quantum numbers are those of the singlet ground state. The theoretical expectation for the value of M^2 including the Breit correction is 3.90. The eigenvalues M^2 seem to be more stable with increasing Λ in the $e^+e^-(\gamma)$ equation than in the LCS equation.

can be kept finite in the continuum limit. Ideally, it should be increased toward larger values after satisfactory convergence with resolutions K and $R_\perp$ has been achieved. Figure 8 with increasing Λ at fixed $R_\perp$ and K is thus considered to be of academic interest and is added for completeness only. From Eq. (21), the value of Λ should neither be too small nor too large at fixed $R_\perp$. One should hope to get approximate independence of Λ for intermediate values of Λ. Looking at Fig. 8(a), one indeed observes that the ground-state eigenvalue of the $e^+e^-(\gamma)$ equation (squares) is approximately independent of Λ on an interval of Λ between 0.6 and 1.0. The eigenvalue varies between 3.916 and 3.921 in this interval. There is no interval of stabilization for the ground-state eigenvalue of the LCS equation (circles), which signals that the mathematical parameter values are not in the regime of absolute independence on parameters for the LCS equation.

In Fig. 8(b), one is tempted to see approximate independence of $\tilde{R}$ on Λ at values of Λ around 0.7, but this is not really the case. One can only observe that the derivative $|\partial\tilde{R}/\partial\Lambda|$ is smallest at Λ around 0.7, for both the $e^+e^-(\gamma)$ and the LCS equation. The value of $\tilde{R}$ at this Λ and $R_\perp$ is reasonable, around $8m^{-1}$.

In Fig. 8(c) we find that $P_{e^+e^-}$ depends strongly on Λ. We attribute this to the fact that $P_{e^+e^-}$ is the probability of finding a pair of bare electron and bare positron in the positronium and this probability should depend on Λ [33].

C. Distribution functions

After having presented the degree of independence of values of M^2, $\tilde{R}$, and $P_{e^+e^-}$ on mathematical parameters, we turn to present the fermion and the photon distribution functions at our best parameter values $R_\perp = 5.99$, $K = 30$ and $\Lambda = 1.0$.

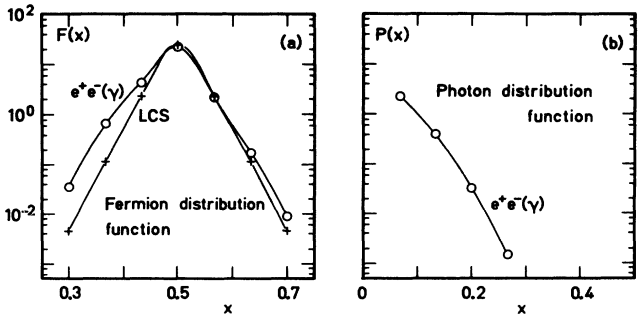

FIG. 9. Fermion and photon distributions of the singlet ground state: (a) Fermion distribution function $F(x)$, see definition in the text; (b) photon distribution function $P(x)$, see definition in the text. Calculations were done with $R_\perp = 5.99$, $K = 30$, $\alpha = 0.3$, $\Lambda = 1.0$ for both the $e^+e^-(\gamma)$ equation (points) and for the LCS equation (crosses). The symmetry quantum numbers are those of the singlet ground state. Note that in comparison with $F(x)$ of the LCS equation ground state, $F(x)$ of the $e^+e^-(\gamma)$ equation ground state is broader and shifted toward lower values of x.

In Fig. 9(a), the fermion distribution function or structure function $F(x)$ is presented for both the $e^+e^-(\gamma)$ equation (circles) and the LCS equation (crosses). Note the logarithmic scale on the abscissa. $F(x)dx$ is a probability to find a charged particle (electron or positron) with a longitudinal momentum fraction within an interval dx around x:

$$F(x) = \sum_{s_1 s_2} \int dy\, d^2k_\perp [\delta(x,y) + \delta(x,1-y)] \mid \psi^{e^+e^-}_{s_1 s_2}(y, k_\perp) \mid^2 + \int dy_1 dy_2 d^2k_{\perp 1} d^2k_{\perp 2} [\delta(x,y_1) + \delta(x,y_2)] \mid \psi^{e^+e^-\gamma}_{s_1 s_2 s_3}(y_1, k_{\perp 1}, y_2, k_{\perp 2}) \mid^2 . \tag{31}$$

In the $e^+e^-(\gamma)$ and in the LCS equation, $F(x)$ is normalized to 2, $\int_0^1 dx F(x) = 2$, since there are two fermions in both e^+e^- and $e^+e^-\gamma$ Fock state types. $F(x)$ for the LCS equation is symmetric about $x = \frac{1}{2}$ and is a bell-shaped curve. One observes close to exponential falloff of $F(x)$ with $|x - \frac{1}{2}|$ for both equations. As compared to $F(x)$ of the LCS equation, $F(x)$ of the $e^+e^-(\gamma)$ equation is depleted at $x = \frac{1}{2}$, broader, and enhanced at low and high values of x. The full width at half maximum of $F(x)$ is about 0.075 for both equations, which is $\alpha/4$ for $\alpha = 0.3$. The expectation value of x, $\langle x \rangle = \frac{1}{2}\int_0^1 dx\, xF(x)$, is shifted from $\langle x \rangle = 0.50$ with the LCS equation toward $\langle x \rangle = 0.49$ with the $e^+e^-(\gamma)$ equation.

In Fig. 9(b), the photon distribution function of positronium $P(x)$ is presented. $P(x)dx$ is the probability to find a photon on an interval dx at given longitudinal-momentum fraction x:

$$P(x) = \sum_{s_1 s_2 s_3} \int dy_1 dy_2 d^2k_{\perp 1} d^2k_{\perp 2} \delta(x, 1 - x_1 - x_2) \times \mid \psi^{e^+e^-\gamma}_{s_1 s_2 s_3}(y_1, k_{\perp 1}, y_2, k_{\perp 2}) \mid^2 . \tag{32}$$

It is normalized to $\int_0^1 dx\, P(x) = 1 - P_{e^+e^-}$. At our parameter values $R_\perp = 5.99$, $K = 30$, and $\Lambda = 1.0$, $P_{e^+e^-} \approx 0.815$, see Fig. 8(c). We have checked that the distribution functions are independent of $R_\perp$ on a 10% level at this point. We have not, however, checked for the degree of independence on K and Λ.

To summarize, we have systematically studied the dependence of the ground-state properties of the $e^+e^-(\gamma)$ and the LCS equation on *all* the mathematical parameters transverse resolution $R_\perp$, longitudinal resolution K, and ultraviolet regulator Λ, at a fixed value of the coupling constant $\alpha = 0.3$. The approximate indepen-

dence (within less than 10%) of the observables invariant mass squared M^2 and charge radius $\tilde{R}$ on mathematical parameters has been found. No sign of unexpected (say, divergent) behavior of the observables M^2 and $\tilde{R}$ when changing the mathematical parameters was found. The results for e^+e^- state probability $P_{e^+e^-}$ were not stable with respect to varying K or Λ. The fermion and the photon distribution functions were presented as well. Wherever the comparison with the LCS equation could be made, a good agreement was found. The first effects of retardation, such as shift of the structure function peak from the value of $x = 0.5$ with the LCS equation toward the values of x below $x = 0.5$ are observed. These effects have probably not been calculated reliably, since the zero modes and the Coulomb singularity were treated on the level of the LCS equation.

V. SUMMARY

The $e^+e^-(\gamma)$ model for positronium has been derived from QED by truncating the particle Fock basis to include just the e^+e^- and the $e^+e^-\gamma$ states. In accord with the truncation, the active part of the light-cone QED Hamiltonian has been determined by consistently employing the gauge principle for the light-cone gauge. In particular, all the instantaneous photon interaction matrix elements between the e^+e^- Fock states and all the instantaneous fermion interaction matrix elements between the $e^+e^-\gamma$ states are included in the calculation. It is not absolutely clear at this point whether the truncation of the Fock basis represents an approximation to the full problem, which in principle includes an infinite number of particles. To investigate this question, one should increase Λ, as well as $R_\perp$ and K and check whether the results converge to a high degree of accuracy. Note that using the regulator of Eqs. (4) and (5), for $R_\perp < 6$ the fermions carry at most 2 units of momentum in each of the perpendicular directions and the photons at most 4 units. The Hamiltonian matrix was constructed blockwise to make use of its sparseness. It was diagonalized efficiently as a sparse matrix using the Bauer-Rutishauser simultaneous iteration algorithm. Use of the exact discrete symmetries reduced the matrix size by roughly a factor of 8 in each symmetry sector. The zero-mode photon singularity as well as the Coulomb singularity have been devoted a special treatment in the $e^+e^-(\gamma)$ model, the same as in the light-cone Schrödinger equation.

At the coupling constant $\alpha = 0.3$, a region of approximate independence of the $e^+e^-(\gamma)$ model ground-state invariant mass squared on all the mathematical parameters was found. The value of the invariant mass squared in this region gives the result for the binding energy. The precision of this result is estimated from the behavior of the eigenvalue as each of the mathematical parameters is varied. The result for the binding energy agrees with the Bohr value within 10%. Slightly worse agreement with the Bohr value was found for the charge radius. The ground-state binding energy and the charge radius of the $e^+e^-(\gamma)$ model ground state agree within less than 10% with the binding energy and the charge radius of the light-cone Schrödinger equation ground state. Novel aspects as compared to the light-cone Schrödinger equation appear in the $e^+e^-(\gamma)$ equation. These include the broadening of the structure function, shift of the structure function peak from $x = \frac{1}{2}$ toward lower values of x and smaller charge radius. The photon distribution function in the $e^+e^-(\gamma)$ model is presented. It is concentrated at low values of x.

One cannot yet be satisfied with the results presented. Nevertheless, it was shown that the $e^+e^-(\gamma)$ approximation is numerically tractable without the need of supercomputers. The unsymmetrized Hamiltonian matrices of dimensions up to 100 000 by 100 000 were constructed and diagonalized using a workstation. The accuracy of the approach of about 10% is worse than that of the effective two-body potential model [15], derived from the $e^+e^-(\gamma)$ model. However, in deriving the effective two-body potential model there are more *ad hoc* assumptions than in the $e^+e^-(\gamma)$ model. The equal-time approaches [23, 24] are even more accurate, but it is difficult to generalize them [23, 24] and it is difficult to calculate the observables, such as structure functions, from the wave functions. At the actual value of the QED coupling constant of $\alpha \approx 1/137$, the traditional state-of-the-art calculations [34, 35] are most accurate. In traditional bound-state methods, a larger set of graphs is used normally as in the $e^+e^-(\gamma)$ model. It would be most useful to compare the methods in detail. This, however, seems premature at present since this paper represents just a first step toward an accurate description using the light-cone techniques. At weak coupling, both types of analysis should give correct results ultimately. The dissadvantage of the present method at weak coupling is that the single momentum-space grid should cover all the different momentum scales present in the problem. It remains to be seen whether or not the light-cone techniques will prove superior at the intermediate or large values of the coupling constant.

As it looks, the $e^+e^-(\gamma)$ model is a sound approximation to the full QED in the sector of positronium. Provided one is strictly led by the gauge principle the divergences characteristic of the light-cone gauge and of the light-cone quantization seem to be absent. The power of the method of DLCQ to provide guidelines, if qualitative, for the subsequent application of more accurate methods, has been exhibited in 3+1 dimensions.

As for the perspectives, there is certainly room for improvement. It is possible to treat the zero-mode photon contribution more precisely in the $e^+e^-(\gamma)$ model, which should improve the convergence properties of the photon distribution function of positronium in the model, as well as of the hyperfine splitting results, not presented in this paper. Advances in numerical techniques are desirable. The known approximate eigenvectors can be used as a starting point to speed up the convergence of the diagonalization routine. A true sparse *complex* matrix diagonalization routine can be constructed. The Lanczos algorithm [3] seems promising for obtaining the ground eigenstate.

The $e^+e^-(\gamma)$ model can be systematically improved in many ways. The resolutions $R_\perp$ and K as well as

regulator Λ can be increased and the finite-size-scaling techniques can be used to extrapolate to even larger values. Further Fock basis states can be included, which would enable studying other effects, such as the Lamb shift. The next possible step is a direct calculation of the QCD bound states, such as heavy quarkonia. In QCD, the nontrivial gluon dynamics will have to be devoted a special attention.

ACKNOWLEDGMENTS

We would like to acknowledge helpful discussions with Stanley Brodsky, Kent Hornbostel, Michael Krautgärtner, and Andrew Tang. One of the authors (M.K.) would like to thank the organizers of the Perturbative QCD Workshop for hospitality in Lund, where a part of this work was done.

[1] H. C. Pauli and S. J. Brodsky, Phys. Rev. D **32**, 1993 (1985).
[2] T. Eller, H. C. Pauli, and S. J. Brodsky, Phys. Rev. D **35**, 1493 (1987).
[3] J. R. Hiller, Phys. Rev. D **43**, 2418 (1991).
[4] A. Harindranath and J. P. Vary, Phys. Rev. D **37**, 3010 (1988).
[5] K. J. Hornbostel, S. J. Brodsky, and H. C. Pauli, Phys. Rev. D **41**, 3814 (1990).
[6] M. Burkardt, Nucl. Phys. **A504**, 762 (1989).
[7] M. Burkardt and R. Busch, in *Particle Physics—The Factory Era*, Proceedings of the Lake Louise Winter Institute, Lake Louise, Canada, 1991, edited by B. A. Campbell, A. N. Kamal, P. Kitching, and F. C. Khanna (World Scientific, Singapore, 1991).
[8] H. C. Pauli and S. J. Brodsky, Phys. Rev. D **32**, 2001 (1985).
[9] R. J. Perry, A. Harindranath, and K. G. Wilson, Phys. Rev. Lett. **65**, 2959 (1990).
[10] G. McCartor, Z. Phys. C **41**, 271 (1988).
[11] Th. Heinzl, St. Krusche, and E. Werner, Phys. Lett. B **256**, 55 (1991).
[12] G. P. Lepage and S. J. Brodsky, Phys. Rev. D **22**, 2157 (1980).
[13] A. C. Tang, S. J. Brodsky, and H. C. Pauli, Phys. Rev. D **44**, 1842 (1991).
[14] A. C. Tang, Ph.D. thesis, Stanford University, Report No. SLAC-351, UC-414, 1990.
[15] M. Krautgärtner, H. C. Pauli, and F. Wölz, Phys. Rev. D (to be published).
[16] M. Kaluža, Ph.D. thesis, University of Heidelberg, 1990.
[17] L. C. L. Hollenberg, K. Higashima, R. C. Warner, and B. H. J. McKellar, Report No. KEK-TH-280, 1991 (unpublished).
[18] S. J. Brodsky, T. Huang, and G. P. Lepage, in *Particles and Fields—2*, Proceedings of the Banff Summer Institute, Banff, Canada, 1981, edited by A. Z. Capri and A. N. Kamal (Plenum, New York, 1983).
[19] G. P. Lepage, S. J. Brodsky, T. Huang, and P. B. Mackenzie, in *Particles and Fields—2* [18].
[20] A. C. Tang, Phys. Rev. D **37**, 3014 (1988).
[21] G. Leibbrandt, Rev. Mod. Phys. **59**, 1067 (1987).
[22] F. Wölz, M.S. thesis, University of Heidelberg, 1990.
[23] W. Dykshoorn, R. Koniuk, and R. Muñoz-Tapia, Phys. Rev. A **41**, 60 (1990).
[24] W. Dykshoorn and R. Koniuk, Phys. Rev. A **41**, 64 (1990).
[25] S. Pissanetsky, *Sparse Matrix Technology* (Academic, London, 1984).
[26] P. J. Nikolai, ACM Trans. Math. Software **5**, 118 (1979).
[27] H. Rutishauser, Numer. Math. **16**, 205 (1970).
[28] J. G. Lewis, Stanford University Technical Report No. STAN-CS-77-595, 1977 (unpublished).
[29] S. D. Drell and T.-M. Yan, Phys. Rev. Lett. **24**, 181 (1970).
[30] J. F. Gunion and D. E. Soper, Phys. Rev. D **15**, 2617 (1977).
[31] J. J. Sakurai, *Modern Quantum Mechanics* (Addison-Wesley, Redwood City, CA, 1985).
[32] B. A. Thacker and G. P. Lepage, Phys. Rev. D **43**, 196 (1991).
[33] C. Itzykson and J.-B. Zuber, *Quantum Field Theory* (McGraw Hill, New York, 1987).
[34] J. R. Sapirstein and D. J. Yennie, in *Quantum Electrodynamics*, edited by T. Kinoshita (World Scientific, Singapore, 1990).
[35] T. Kinoshita and D. R. Yennie, in *Quantum Electrodynamics* [34].